ELSEVIER

Biomaterials 23 (2002) 4739–4751

Biomaterials

www.elsevier.com/locate/biomaterials

A three-dimensional osteochondral composite scaffold for articular cartilage repair

Jill K. Sherwood[a,*], Susan L. Riley[b], Robert Palazzolo[a], Scott C. Brown[a], Donald C. Monkhouse[a], Matt Coates[c], Linda G. Griffith[c], Lee K. Landeen[b], Anthony Ratcliffe[b]

[a] *Therics, Inc., 115 Campus Drive, Princeton, NJ 08540, USA*

[b] *Advanced Tissue Sciences, Inc., 10933 N. Torrey Pines Road, La Jolla, CA 92037, USA*

[c] *Department of Chemical Engineering and Division of Bioengineering & Environmental Health, Massachusetts Institute of Technology, 66-466 25 Ames St, Cambridge, MA 02139, USA*

Received 16 May 2002; accepted 30 May 2002

Abstract

There is a recognized and urgent need for improved treatment of articular cartilage defects. Tissue engineering of cartilage using a cell-scaffold approach has demonstrated potential to offer an alternative and effective method for treating articular defects. We have developed a unique, heterogeneous, osteochondral scaffold using the TheriForm™ three-dimensional printing process. The material composition, porosity, macroarchitecture, and mechanical properties varied throughout the scaffold structure. The upper, cartilage region was 90% porous and composed of D,L-PLGA/L-PLA, with macroscopic staggered channels to facilitate homogenous cell seeding. The lower, cloverleaf-shaped bone portion was 55% porous and consisted of a L-PLGA/TCP composite, designed to maximize bone ingrowth while maintaining critical mechanical properties. The transition region between these two sections contained a gradient of materials and porosity to prevent delamination. Chondrocytes preferentially attached to the cartilage portion of the device, and biochemical and histological analyses showed that cartilage formed during a 6-week in vitro culture period. The tensile strength of the bone region was similar in magnitude to fresh cancellous human bone, suggesting that these scaffolds have desirable mechanical properties for in vivo applications, including full joint replacement.

Keywords: TheriForm; Three-dimensional printing; Cartilage; Osteochondral; Tissue engineering; PLGA; Osteoarthritis

1. Introduction

Over 16 million people in the US suffer from severe joint pain and related dysfunction, such as loss of motion, as a result of injury or osteoarthritis [1,2]. In particular, loss of function of the knees can severely impact mobility and thus the patient's quality of life. The biological basis of joint problems is the deterioration of articular cartilage [3], which covers the bone at the joint surface and performs many complex functions. Articular cartilage is composed of hyaline cartilage which has unique properties, such as viscoelastic deformation, that allow it to absorb shock, distribute loads, and facilitate stable motion [4–13]. Self-repair of hyaline cartilage is limited [14,15] and the tissue that forms is usually a combination of hyaline and fibrocartilage [16], which does not perform as well as hyaline cartilage and can degrade over time [17].

Current treatments for articular defects have limited success in that they are deficient in long-term repair or have unacceptable side effects. Autograft procedures, such as Mosaicplasty [18] and Osteochondral Autograft Transfer System (OATS) [19], remove an osteochondral plug from a non-load bearing area and graft it into the defect site. Despite the recent successes this procedure has seen in repairing cartilage lesions, it requires additional time and money to acquire the donor tissue and results in donor site morbidity and pain [20]. Carticel®, a procedure consisting of injecting cells under a periosteal flap, has also had limited success; however, the procedure lacks inter-patient consistency with some

*Corresponding author. Schering-Plough Research Institute, 2000 Galloping Hill Road, K-11-2 J5, Kenilworth, NJ 07033, USA. Tel.: +1-908-740-2549; fax: +1-908-740-2802.

E-mail address: jill.sherwood@spcorp.com (J.K. Sherwood).

0142-9612/02/$ - see front matter
PII: S0142-9612(02)00223-5

patients maintaining little relief months or years later, and the surgical procedure is technically challenging. Abrasion arthroscopy, subchondral bone drilling and microfracture typically result in fibrocartilage filling the defect site. Allogenic transplantation of osteochondral grafts has had clinical success, but supply is limited and has a risk of infection [16,21–24].

Each of the currently used repair modalities has severe limitations [25–29], and the outcome is generally regarded as inadequate. Tissue engineering of cartilage has great potential in providing the appropriate replacement tissue with features necessary for a successful repair of cartilage to occur. While there has been success in growing cartilage in vitro, success in vivo requires reliable fixation into the joint defect and integration with the subchondral bone. Ultimately, for defects in articular locations with substantial curvature, the tissue-engineered constructs should also have appropriate topography. We propose using a fully resorbable synthetic scaffold, containing a cartilage region and a bone-appropriate region made by the TheriForm™ three-dimensional printing process, in a cell-scaffold-based tissue engineering approach to repair articular defects [30–32]. In the TheriForm process, scaffolds are built one thin layer at a time, which allows for the production of multiphasic devices, and has the capability to fabricate devices with biologically and anatomically relevant features. The primary features of these scaffolds are: (1) a highly porous cartilage region to facilitate seeding chondrocytes selectively in this region, (2) staggered channels in the cartilage region to promote homogeneous seeding throughout the 2-mm thickness of the region [33], (3) a cloverleaf bone region to promote bone ingrowth for fixation and integration while maintaining necessary mechanical characteristics, and (4) a transition region with a gradient of materials and pore structure to prevent delamination. Autologous chondrocytes that have been expanded in culture from a small biopsy or expanded allogenic chondrocytes that have been extensively tested for diseases can then be seeded onto the top portion of the scaffold [34,35]. A significant amount of work has been published on the interactions of chondrocytes and resorbable polymers [36–40]. The seeded scaffold can then be cultured in vitro until adequate tissue formation has occurred and then implanted into the cartilage defect site [41].

In this paper we describe studies aimed at: (1) the selection of the appropriate polymeric material for the cartilage region, (2) mechanical testing of the bone region including the effect of porosity and polymer/calcium phosphate ratio, (3) prevention of delamination in the transition region, and (4) selection of an appropriate chondrocyte seeding method that results in high matrix deposition in the cartilage region but little in the bone region.

2. Materials and methods

2.1. Solvent casting and testing of thin films

To initially screen polymer combinations and molecular weights, thin films were cast. In 7-ml glass scintillation vials, 200 mg of polymer (as received) was dissolved in 2 ml of chloroform. The solutions were mixed and placed on an orbital shaker until the polymer completely dissolved. The solutions were mixed again immediately before being poured into a 6-cm diameter glass Petri dish. The films were allowed to dry covered and undisturbed for 48 h in a laminar flow hood. After drying, the films were peeled from the bottom of the dishes and statically incubated in phosphate buffered saline (PBS) at 37°C for three weeks. A sample was taken and qualitatively evaluated once weekly for color (e.g., clear or white), rigidity (e.g., brittle or flexible), structural integrity (e.g., tears, crumbles, or remains intact when collecting a sample), and amount of degradation (e.g., partially or completely degraded).

2.2. Powder preparation

Polymer powders were cryogenically milled in an ultra-centrifugal mill (Model ZM 100; Glen Mills, Clifton, NJ) with liquid nitrogen. The powders were vacuum-dried and hand-sieved with stainless steel sieves (W.S. Tyler Co., Mentor, OH). NaCl was prepared by milling in a large analytical mill (Model A20; Janke and Kunkel GmbH, Germany) at 20,000 rpm and sieved to the specified range within 106–150 μm. Calcium phosphate tribasic (TCP; Sigma, St. Louis, MO) was sieved to 38–106 μm as received. The powders were sieved using Retsch screens (Retsch, Haan, Germany) along with zirconia milling media. The stack of screens was placed on a vibrating sifter-shaker (Retsch) and shaken for 15 min to separate the powders based on particle size. The powders were mixed on a ball mill (US Stoneware, East Palestine, OH).

2.3. Scaffold fabrication using the TheriForm™ process

The TheriForm™ process is CAD/CAM driven and selectively binds powder particles with a liquid binder to form solid three-dimensional objects one layer at a time, as described elsewhere [42–45]. Briefly, external shapes (e.g., cloverleaf) and internal architectural features (e.g., channels) are created via CAD software. During fabrication, a thin layer of powder (polymer/NaCl or polymer/NaCl/TCP) was spread on a piston plate and a printhead rastered above the powder bed and deposited chloroform (Fisher Scientific, Pittsburgh, PA) droplets in selective areas to create the scaffold (see Fig. 1). After one layer was complete, the piston plate was lowered and a new layer of powder was spread, followed by

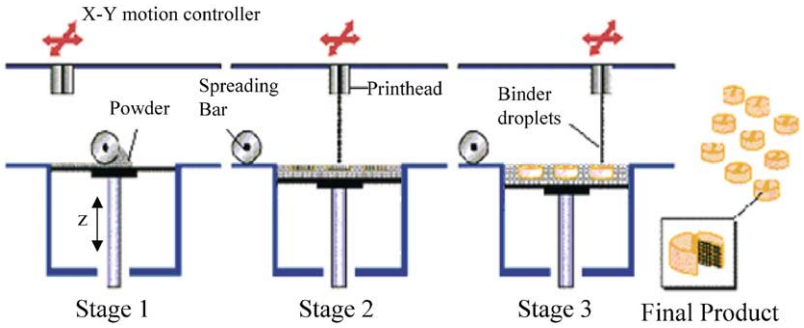

Fig. 1. The TheriForm fabrication process. A laminated process in which a thin layer of powder is spread and then bound together in desired areas with a liquid binder.

additional deposition of binder (chloroform). The lamination process was iterated until fabrication was complete. The fabrication of these research-grade prototypes was aided by the use of templates for the outer shape (e.g., cloverleaf). The plate of parts was dried overnight at room temperature and the loose powder was removed to reveal the final scaffolds. Residual chloroform was removed with liquid CO_2 and the NaCl was leached to create the micro-pores, as described below.

2.4. Solvent extraction using liquid CO_2

Samples were loaded and sealed into the extractor chamber (Marc Sims S.F.E., Berkeley, CA). The system was filled with liquid CO_2 and pressurized to 4000 psi. The system was held for approximately 10 min and was vented for 10 min at constant pressure. The typical venting rate was 5 standard cubic feet per minute (scfm). The venting-down phase was then initiated. This process was repeated twice per batch.

2.5. NaCl leaching

After removal of residual chloroform, samples were placed into a Nalgene® bottle that contained a minimum of 20 ml of water per sample. The bottle was placed onto an orbital shaker (model 3527, Lab-Line Environ, Melrose Park, IL) at 100 rpm and 37°C or room temperature. The water was replaced every hour. After 5 h, the NaCl content in the solution was checked by adding a few drops of 0.1 N silver nitrate (observation of a white precipitate indicated presence of NaCl). If NaCl was detected, leaching was continued until none was detected (~9 h). Samples were removed, blotted dry, and placed into a vacuum desiccator overnight to complete drying.

2.6. Residual solvent analysis

Residual chloroform analysis was performed by gas chromatography using a flame ionization detector (GC-FID, Shimadzu GC-14, Shimadzu Instruments, MD). The method was based on the USP Organic Volatile Impurities method ⟨641⟩ and used a Rtx-1301 wide-bore glass column (Restek, 30 m long, 0.53 mm ID, 3.0 μm film thickness) with helium as the carrier gas. An independent party (Galbraith Laboratories, Knoxville, TN) verified the amount of residual chloroform in one batch.

2.7. Scanning electron microscopy analysis

An outside laboratory (Evans East, Plainsboro, NJ) performed the scanning electron microscopy (SEM) analysis of polymer scaffolds. The scaffolds were carefully sectioned along the channels with a razor blade and mounted onto aluminum stubs. Prior to examination, each sample was gold coated. A JEOL 5300 SEM microscope at 20 kV was used to perform image analysis. Polaroid micrographs were taken of both surface and cross-sectional views of each sample.

2.8. Mechanical testing of the bone region

The mechanical properties of the bone portion of the osteochondral device were investigated by performing mechanical testing on dog bone-shaped and cylindrical parts made of L-PLGA(85:15), TCP, and NaCl using the TheriForm process. The TCP was used in the 38–150-μm particle size range, and NaCl (Fisher) in the 75–150-μm size was used. Samples of five different compositions were fabricated to study the influence of porosity and inorganic content on tensile and compressive properties. The tensile specimens were twenty 200-μm layers thick, and the compression samples were sixty 200-μm layers. Samples were liquid CO_2-dried to remove residual chloroform, leached (200 ml water per sample) for 15 h (changing the water every 5 h) and dried for 48 h in a vacuum oven (at 1 bar) at room temperature before testing.

Determination of values for elastic modulus, yield strength, tensile strength, percent elongation and compressive strength were obtained from load-displacement

curves, briefly described below. Tensile testing specimens were fabricated with dimensions conforming to ASTM standard D 638-96. An Instron Testing machine (model 4201, Instron, Canton, MA) was used for both tensile and compression testing. Pneumatic grips (Instron type 2712) were used to hold the specimens in place with an external air pressure of 30 psi. This pressure produced some deformation of the wide section of the sample. To ensure good transfer of load from the grips to the specimen, it was necessary to use a spacer on the far edge of the grips. A strain rate of 0.1 mm/min was applied on five replicates and the load was recorded during the process. Displacement was measured using extensometers (Instron, Cat. no. 2620–826, travel ± 0.254 mm) with plasticine underneath. The elastic modulus was calculated as the ratio of stress to strain before the material yielded, using the initial cross-sectional area in the calculations. Tensile strength was found as the peak stress before fracture.

Compression testing was carried out according to the ASTM standard D 695-96. This protocol recommended using a cylindrical specimen with a length twice its diameter. Cylindrical samples were fabricated having diameters of 6 mm and lengths of 12 mm for use in this study. Five replicates of each composition were subjected to this test using the same Instron as for the above tensile tests. After removing surface aberrations using fine sandpaper, the samples were placed between the faces of a compression plate on the top and a compression anvil on the bottom (Instron, cat. no. 2501-107 for the upper plate, 2501-085 for the lower anvil). Compression was carried out to between 7% and 20% strains at a rate of 0.5 mm/min. In most cases, the specimen was unloaded in a controlled manner and the hysteresis recorded. Uniform deformation was assumed. The initial cross-sectional area was used in the following calculations. The compressive strength was defined as the point at which lines from the initial linear region and terminal linear region intersected. The elastic modulus was calculated as the ratio of stress to strain or the slope of the initial linear region of a stress versus strain plot, using the initial cross-sectional area in the calculations.

2.9. Determination of shrinkage

The shrinkage of scaffolds was determined by measuring the diameter and/or thickness of the scaffold with a micrometer. The measurements were taken at several time points during leaching, while the scaffolds were still wet.

2.10. Seeding of scaffolds

The seven batches of disk scaffolds that were evaluated for the cartilage region were screened for their ability to support cellular attachment, cellular colonization, and matrix deposition using dermal fibroblasts as a representative attachment-dependent and matrix-synthesizing cell type. Scaffolds were pre-wetted in ethanol (70%) for 1 min, disinfected in antibiotic/antimycotic (20X concentration; Gibco, Gaithersburg, MD) overnight and pre-treated in culture medium (Dulbecco's Modified Eagle medium [DMEM; Gibco], supplemented with bovine calf serum [10%; Hyclone, Logan, UT], sodium pyruvate [Gibco], non-essential amino acids [Gibco], L-glutamine [Gibco], and antimicrobial agents [Gibco]) overnight. Each disk was seeded for 18–24 h with 1×10^6 dermal fibroblasts in 500 μl of culture medium under gentle agitation. The disks were cultured statically in culture medium supplemented with ascorbate (50 μg/ml; Baker, Phillipsburg, NJ) for 4 weeks in 37°C, 5% CO_2, humidified incubators.

Osteochondral devices were either cultured rotationally by submerging in a tube or top-seeded by pipetting the cells onto the top of the scaffold. Before seeding with chondrocytes, the devices were first pre-wet in ethanol (100%) for 15–60 min. The ethanol was removed by rinsing in PBS three times (5–10 min each rinse on a shaker) and the scaffolds were soaked overnight in antibiotic/antimycotic solution to disinfect. The scaffolds were placed in DMEM medium containing 10% fetal bovine serum (FBS, Hyclone) and 25 μg/ml gentamicin sulfate (GS) (Gibco) for four hours prior to seeding. Scaffolds that were rotationally seeded were placed in a 15-ml conical centrifuge tube that contained 15×10^6 ovine articular chondrocytes (OAC) from the femoral condyle and filled full with the above medium. The scaffolds were rotated end-over-end overnight in an incubator. For scaffolds that were top-seeded, 15×10^6 OAC were concentrated in 250 μl and pipetted on top of the constructs placed in the wells of 6-well plates. The top-seeded scaffolds were left undisturbed for 3.25 h to allow for the cells to settle and attach to the scaffolds, after which time more medium was added to the wells to prevent desiccation. Both sets of scaffolds were cultured statically in 6-well plates for 4 weeks in 37°C, 5% CO_2, and humidified incubators.

2.11. Biochemical analyses

Biochemical analyses were performed at 1, 2, 3 and 4 weeks for the final seven candidate systems and after 4 weeks in culture for the osteochondral scaffolds.

2.11.1. MTT

Estimation of cellular activity and spatial distribution was accomplished using the MTT assay. MTT (3-[4,5-Dimethylthiazol-2-yl]-2.5-diphenyltetrazolium bromide) is a dye that measures cell activity and is taken up by the

mitochondria and converted to a blue color for viable and metabolically active cells. Briefly, samples were incubated in MTT solution (0.5 mg/ml in 2% fetal bovine serum culture medium) (Sigma) for 2 h and rinsed with PBS for 5–10 min. The insoluble precipitant was extracted in isopropanol (5 ml) for 24 h at room temperature, and the optical density (OD) was determined at 540 nm. Linear correlations between OD and cell numbers were previously established (unpublished results).

2.11.2. DNA/cell number

The total amount of DNA was determined utilizing a Hoechst 33258 dye (Molecular Probes, Eugene, OR) method [46–48] that was modified for use in a microtiter plate reader. Briefly, samples were digested overnight at 37°C in papain solution (1 mg/ml in PBS; Sigma) and reacted with Hoechst dye (0.5 μg/ml) in the dark for 30 min at room temperature. After incubation, fluorescence was quantified using a plate reader (Cytofluor®, Persceptive Biosystems, Inc., Framingham, MA) and concentrations were determined against a standard curve made from bovine thymus DNA. Cell numbers were calculated using the estimated value for cellular DNA content of 7.7 pg DNA/cell.

2.11.3. GAG

Sulfated glycosaminoglycans (S-GAG) were determined spectrophotometrically by a method [47–50] adapted for use with a microtiter plate reader. Briefly, aliquots of the papain-digested sample solution (see DNA section above) were mixed with 1,9 Dimethylmethylene blue (DMMB; Aldrich, Milwaukee, WI) dye solution and read on a plate reader (Molecular Devices, Sunnyvale, CA) with a dual wavelength setting of 540/595 nm. A standard curve was generated using chondroitin-4-sulfate (Sigma) and used to determine the concentration of S-GAG in the samples.

2.11.4. Collagen

Total collagen was indirectly determined spectrophotometrically by the presence of hydroxyproline by a method [51] adapted for use with a microtiter plate reader. Briefly, aliquots of the papain-digested sample solution (see DNA section above) were hydrolyzed with concentrated hydrochloric acid (6 N), dried, and resuspended in a sodium phosphate buffer, pH 6.5. The presence of hydroxyproline was detected by an oxidation reaction with chloramine T/P-DAB at 60°C for 30 min. A standard curve was generated using L-hydroxyproline and used to determine the concentration of hydroxyproline in the samples. The calculation of collagen content was based on the estimated percent of hydroxyproline in collagen of 14.3%.

2.12. Histology

Histological specimens were fixed in 10% neutral buffered formalin and processed for either paraffin or plastic embedding. Plastic-embedded samples were catalyzed in glycol methacrylate and allowed to polymerize at room temperature for approximately 1 h. The blocks were sectioned using an automated microtome, and sections (3–4 μm in thickness) were mounted on glass slides. After drying for approximately 1 h at room temperature, the slides were stained with hematoxylin and eosin or safranin-O to visualize cell and tissue components by light microscopy.

2.13. Statistical methods

One-way analysis of variance (ANOVA), using commercially available statistical software, Sigma Stat, was performed to determine whether significant differences existed between the biochemical results. Post-hoc Tukey testing or Dunn's method (for data sets that failed the normality or equal variance testing) were used for subsequent pairwise comparisons.

3. Results

3.1. Materials selection for the cartilage region

Solvent-cast thin films were qualitatively evaluated over 3 weeks for rates of degradation and structural integrity to narrow the polymer combinations down to seven final candidates. Films were eliminated if they crumbled or tore easily. In addition, flexible materials were viewed as preferable over rigid materials. At 3 weeks, the goal was to have the film mostly degraded so films that did not show significant degradation were eliminated. Seven candidate polymer combinations were chosen by this process and were then fabricated into three-dimensional scaffolds, and tested in vitro for cell attachment and infiltration using dermal fibroblasts as a test cell type (see Table 1). Analysis of the constructs for MTT and DNA showed the highest levels for polymer combinations 1, 4 and 5 and the lowest for combination 7 (see Fig. 2). Two of the candidates (6 and 7) could not tolerate the residual solvent removal process (i.e., pores collapsed) and were eliminated. One combination (3) was too fragile to be fully tested and was ruled out. Combinations 4 and 6 both deformed significantly (i.e., curled) after 4 weeks in culture. Gross morphology and histology indicated that candidates 2, 4, 6, and 7 had tissue development primarily on the surface of the device (see Fig. 3). In contrast, candidates 1 and 5 supported cell attachment and viability, and matrix deposition throughout the cartilage region and maintained the original shape of the scaffold. Candidate 1 was chosen

Table 1
Seven final polymer combinations

Polymer combo	Weight (%)	Polymer (dl/g)	Weight (%)	Polymer (dl/g)
1	50	PLGA(50:50) I.V. 0.48	50	L-PLA I.V. 0.34
2	50	PLGA(50:50) I.V. 0.48 (acid)	50	L-PLA I.V. 0.34
3	50	PLGA(75:25) I.V. 0.24	50	L-PLA I.V. 0.34
4	70	PLGA(50:50) I.V. 0.18 (acid)	30	L-PLA I.V. 0.99
5	70	PLGA(50:50) I.V. 0.48	30	L-PLA I.V. 0.99
6	100	PLGA(50:50) I.V. 0.48	—	—
7	100	PLGA(75:25) I.V. 0.6	—	—

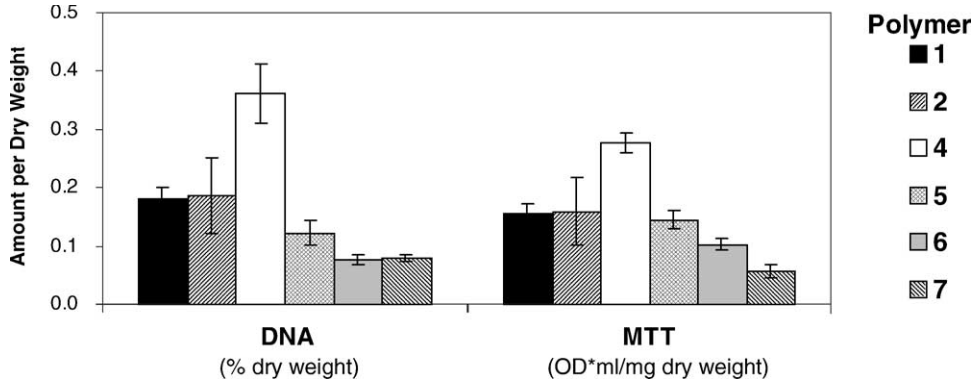

Fig. 2. Biochemical results of TheriForm^{TM} scaffolds created with polymers 1–7 and cultured statically with dermal fibroblasts for 4 weeks. DNA and MTT values were significantly greater for polymer 4 ($p<0.05$, one-way ANOVA with Tukey post-hoc testing). Bars represent mean $\pm$ standard deviations for $n=3$, except for polymer 4 ($n=2$) and the DNA results for polymer 7 ($n=2$).

over 5 because 5 contained a higher molecular weight L-PLA that would likely take longer to resorb than was considered desirable.

3.2. Mechanical testing of the bone region

A set of scaffolds in which the composition of L-PLGA (85:15), NaCl, and TCP were systematically varied was tested for mechanical properties. The results of some of the mechanical tests are reported in Table 2. The general observations were as follows:

1. increasing porosity (or increasing percent of NaCl) decreased the elastic modulus, tensile strength, and yield strength;
2. increasing polymer content (i.e., increasing polymer/TCP ratio at a constant porosity) increased the strength and elastic moduli;
3. specimens with a higher fraction of TCP tended to exhibit brittle fracture under tension, and samples with a lower fraction of TCP displayed ductile rupture;
4. increasing the TCP content decreased the percent elongation to failure (results not shown).

The bone portion was designed with a lower porosity (55%) than the cartilage region (90%) to give this section more mechanical strength. Choosing a porosity for the bone region required balancing mechanical properties, which are closer to bone at low porosities, and high surface area, which promotes vascularization and bone ingrowth and increases with increasing porosity. An interconnected pore structure was desirable for bone ingrowth and requires a minimum of 32% porosity to be fully interconnected according to percolation theory (assuming a simple cubic lattice) [53]. Mechanical properties started to decline around 55% porosity and therefore 55% was thus chosen as the upper acceptable limit. Current bone repair products such as Interpore-200 and Medpor have porosities in the 50–65% range [54,55]. Cancellous bone, which is used for autografts and allografts, has a porosity of 50–90% [56]. Thus, 55% was chosen as the porosity of the bone region. Additionally, a large pore size was used ($>125\,\mu m$) in the bone region to further facilitate mineralized bone ingrowth [57,58] and mechanical strength. Since in vivo bone ingrowth is a gradual process, unlike in vitro cell seeding which occurs at a given instant in time, the low porosity prevented chondrocyte attachment in the bone region during seeding [59], as desired, but is anticipated to allow bone ingrowth in vivo. In addition, during bone ingrowth, the porosity will increase with resorption, facilitating bone ingrowth.

3.3. Architecture of the bone region

In addition to the mechanical properties of the bone portion of the device, the overall outer shape of the device was specifically designed to address several issues. The bone portion was constructed in a cloverleaf shape to specifically:

1. allow the migration of blood and bone marrow-borne tissue forming elements;
2. maximize the surface-area-to-volume ratio to promote bone ingrowth;
3. maximize compressive and torsional strength (to withstand implantation);
4. minimize the amount of polymer (to minimize the cost of device and possible inflammatory response, and promote homogeneous bone formation);
5. be easy to fabricate.

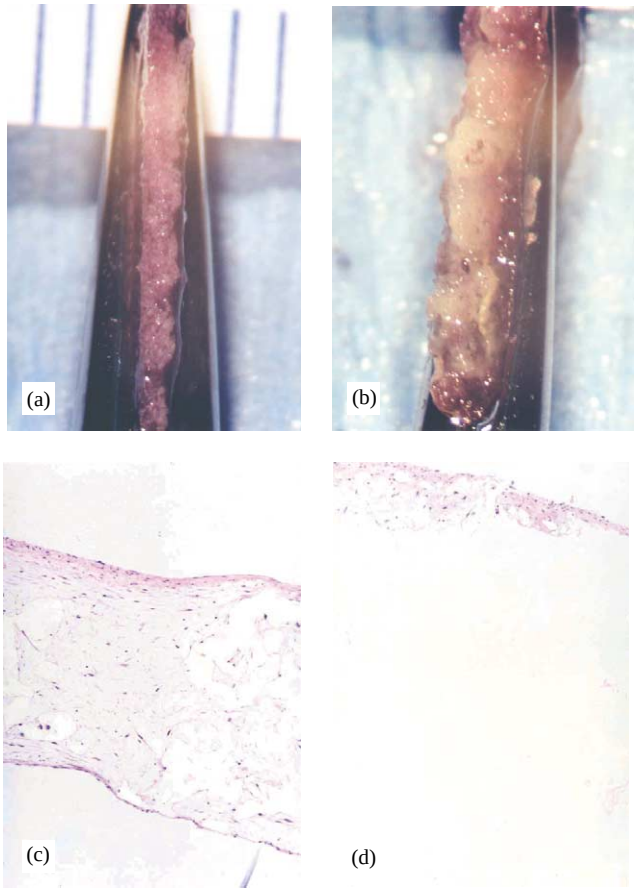

Fig. 3. Cross-sectional views of cultured scaffolds after staining with MTT (a, b) and histological sections after staining with H&E (c, d; 10× objective) of polymer combination 1 (a, c) and combination 4 (b, d). Cells infiltrated the full thickness of combination 1 but were primarily on the surface on scaffold 4.

Several different shapes were considered, including a hollow cylinder and a honeycomb structure. Balancing the variables above, the cloverleaf shape was selected as this would provide mechanical rigidity and allow for a reasonable amount of bone integration.

3.4. Prevention of delamination in the transition region

When the first prototype scaffolds were manufactured, it was discovered that during exposure to prolonged leaching (>24 h), delamination occurred between the cartilage and transition regions. The cause of the delamination was attributed to a significant level of differential shrinkage between these two regions. The adjacent transition region was found to shrink 3.8% in diameter compared to 8.3% for the cartilage region. This caused excessive shear stress and may have been responsible for the delamination.

A study was performed to investigate the parameters suspected to cause shrinkage and to improve the structural integrity of the composite scaffolds. Some of the results as shown in Fig. 4 included:

1. the use of PLGA(50:50) with free acidic side chains increased shrinkage versus regular PLGA(50:50);
2. scaffolds containing 90% NaCl shrank more than those with 85% NaCl;
3. macroscopic channels decreased shrinkage when scaffolds were liquid CO_2 treated;
4. removing residual solvent with liquid CO_2 reduced shrinkage;

Table 2
Tensile and compressive testing data. Averages and standard deviations for $n = 3$ or 4

Composition			Tensile data		Compressive data	
NaCl (%)	TCP (%)	L-PLGA (%)	Tensile strength (MPa)	Elastic modulus (MPa)	Yield strength (MPa)	Elastic modulus (MPa)
25	25	50	5.7±1.0	200±57	13.5±0.3	233±26
35	15	50	5.5±0.8	233±27	13.7±0.8	450±79
35	21.7	43.3	3.3±0.4	180±14	6.5±0.2	184±12
40	15	45	4.0±0.5	183±35	7.0±0.9	180±50
55	11.25	33.75	1.6±0.2	83±18	2.5±0.1	54±17
Cancellous human bone (fresh) [52]			~8	~700–1000	10–20	

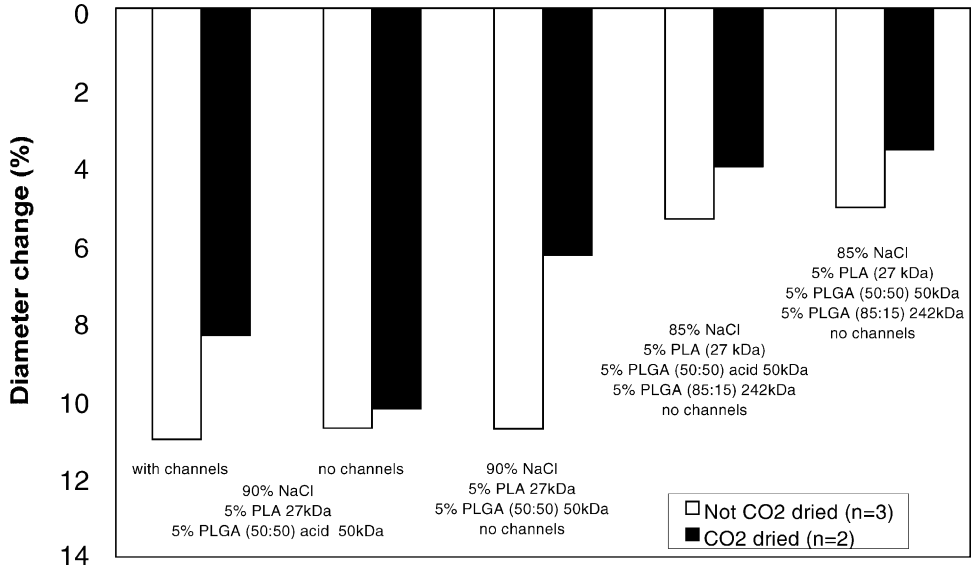

Fig. 4. Amount of shrinkage of scaffolds after leaching for 48 h.

Additional results of the study included (results not shown):

1. scaffolds composed of crystalline L-PLA with an inherent viscosity (I.V.) of 1.1 dl/g and 75% or 90% NaCl shrank less than 2%;
2. shrinkage increased with increasing leaching time;
3. leaching at room temperature reduced shrinkage compared to leaching at 37°C;
4. shrinkage occurred during the leaching phase and not afterwards during drying;

By using a gradient of materials and porosity to slowly change from one material system to the other, delamination was overcome. It was also found that removing the residual chloroform before leaching reduced shrinkage, since the solvent can act as a plasticizer. The addition of macroscopic channels slightly decreased shrinkage of CO_2 dried scaffolds, a distinct advantage since the channels enhance cell seeding in the cartilage region.

3.5. Final osteochondral scaffold composition and design

The osteochondral scaffolds consisted of three distinct regions (see Fig. 5 and Table 3). The bone region was 4.4 mm high and fabricated with 33.75 wt% L-PLGA(85:15) I.V. 1.45 dl/g (Birmingham Polymers Inc., Birmingham, AL) milled to 38–150 μm, 11.25 wt% TCP (Sigma) 38–106 μm, and 55 wt% NaCl (Fisher) 125–150 μm. The bone region was shaped as a cloverleaf. The cartilage region was 2 mm tall and fabricated with 5 wt% D,L-PLGA(50:50) I.V. 0.48 dl/g (Boehringer Ingelheim, Germany) and 5 wt% L-PLA I.V. 0.34 dl/g (Birmingham Polymers Inc.), both milled to 63–106 μm, and 90 wt% NaCl that was 106–150 μm. Staggered channels that were approximately 250 μm were incorporated into the cartilage region. The transition region (1.2 mm) consisted of three sections: 65, 75, and 85 wt% NaCl with 30 wt%, 15, and 5 wt% L-PLGA(85:15), respectively. The balance of the transition sections was composed of a 1:1 ratio of D,L-PLGA (50:50) and L-PLA.

3.6. Seeding of the osteochondral device—selective cell attachment

Top and rotational seeding were investigated to determine the best method to facilitate chondrocyte attachment and proliferation in the cartilage region and prevent chondrocytes from adhering to the bone region. Chondrocytes preferentially seeded into the cartilage portion of the device (Fig. 6) and cell attachment to the bone region was minimal.

Although the same number of cells per scaffold were seeded in both methods, the top seeding method resulted in higher cell, S-GAG, and collagen contents than rotational seeding owing to the higher cell concentration with the top-seeded method (in 0.25 ml) compared to the rotational method (in 15 ml) (see Figs. 7 and 8). The chondrocytes seeded and proliferated homogeneously throughout the 2-mm thickness of the cartilage region due to the high porosity and staggered channel design. Histological analysis showed that after 4 weeks in culture, the chondrocytes had populated the cartilage scaffold and deposited an extracellular matrix containing glycoaminoglycans (as detected by safranin-O staining), as has been seen in other tissue-engineered cartilage constructs [48,50].

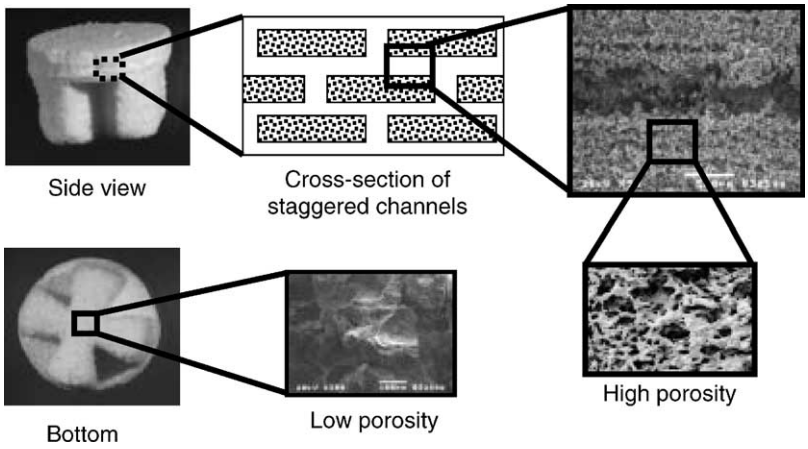

Fig. 5. The osteochondral scaffold has staggered channels in the 90% porous cartilage region to facilitate homogeneous seeding and has a cloverleaf bone region to promote bone ingrowth in vivo. The bone region is 55% porous.

Table 3
Composition of osteochondral scaffold

Region	Amount of NaCl (wt%)	Size of NaCl (μm)	PLGA(50:50) (wt%)	PLA (wt%)	PLGA(85:15) (wt%)	TCP (wt%)
Cartilage	90	106–150	5	5	—	—
Transition 1	85	106–150	5	5	5	—
Transition 2	75	106–150	5	5	15	—
Transition 3	65	106–150	2.5	2.5	30	—
Bone	55	125–150	—	—	33.75	11.25

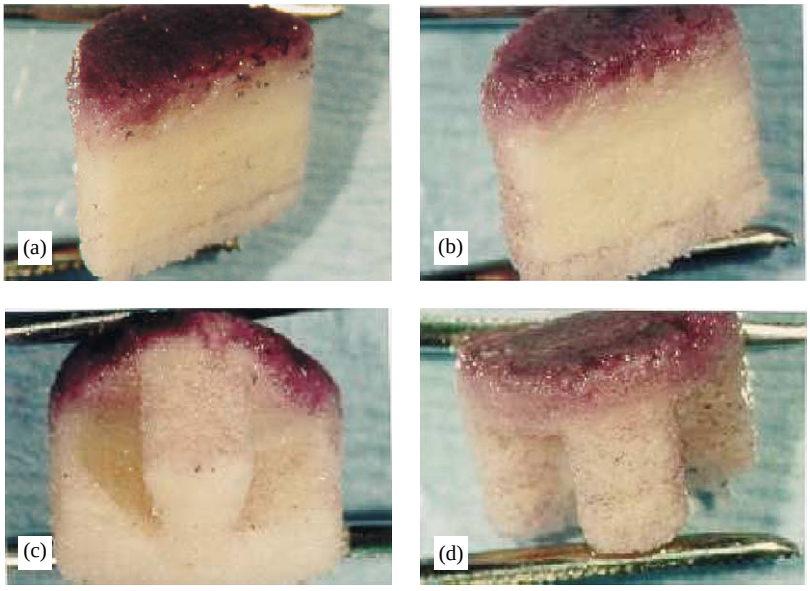

Fig. 6. Cross-sectional view and outer view of MTT stained osteochondral scaffold 24 h after a top seeding (a, c) and after a rotational seeding (b, d) method with OAC from the femoral condyle. Although the entire scaffold was exposed to chondrocytes in the rotational seeding method, the cells preferentially attached to the porous cartilage region, as desired.

4. Discussion and conclusions

We have designed and tested a unique cartilage-bone composite scaffold. This device has two distinct regions (cartilage and bone) composed of different materials, porosity, pore sizes, architectures, and resulting mechanical properties, each specifically optimized for either cartilage or bone. Fabricating a device with two such

varying properties without delamination (i.e., splitting apart) was possible by using a gradient of materials via the laminated three-dimensional TheriForm process.

The candidates of polymer combinations for the cartilage region were first screened by qualitatively evaluating the degradation of solvent-cast films in PBS at 37°C for 3 weeks to select seven candidate polymer combinations. To facilitate cell attachment, proliferation, and matrix deposition, 90% porosity (based on previous studies [59]) and staggered channels were used in the cartilage region. The remaining candidates were fabricated into scaffolds similar to the cartilage region and cultured with dermal fibroblasts for up to 4 weeks and evaluated by gross morphology, biochemical analyses and histology. From these results, a 1:1 ratio of D,L-PLGA(50:50) I.V. 0.48 dl/g and L-PLA I.V. 0.34 dl/g was selected. The seeding method and extent of matrix deposition was determined with the full osteochondral scaffold design. The best cell seeding method was found to be a top seeding approach.

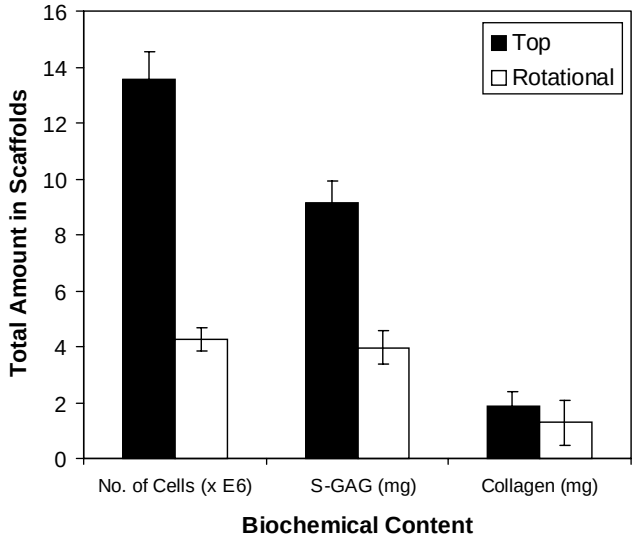

Fig. 7. Biochemical results for TheriForm™ osteochondral scaffolds that were seeded with OAC cells by a top or rotational seeding method and cultured statically for 4 weeks. The top seeding method resulted in greater number of cells and S-GAG content in the scaffolds ($p<0.001$). Collagen content was not statistically different for the two seeding methods and was most likely due to the large standard deviation of the rotational seeded samples. Bars represent mean ± standard deviations for $n=3$.

Results from preliminary mechanical testing of the bone region showed some expected trends. Both the tensile and compressive strengths decreased as the porosity (i.e., void fraction) in the scaffolds increased from 25% to 55%. Likewise, the elastic modulus generally decreased with increasing void fraction. Under ideal conditions, one expects values of the elastic modulus obtained by tensile testing to correspond to the values of the elastic modulus obtained by compression testing. Often, values obtained by compression testing are slightly higher due to friction from the plates. In the samples tested here, it was striking that such agreement was obtained (with the exception of the 35% NaCl:15% TCP:50% PLGA specimen) between the two different methods. This agreement was especially significant because the orientation of the devices during fabrication was not the same in the samples used for each test. Tensile testing was carried out with samples built so that layers were aligned with the direction of strain, while the compression samples were built so that the layers were aligned normal to the direction of strain. Values for the tensile strength of these devices are comparable to the tensile strength of cancellous bone and values for the compressive strength are within an order of magnitude of the compressive strength of cancellous bone (Table 2). Even though scaffolds generated with porosities lower than 55% were stronger than scaffolds generated with a porosity of 55%, the porosity of the bone region was chosen to be 55% (with a pore size of $>125\,\mu m$) to balance strength with the potential for in vivo bone ingrowth. The mechanical testing results suggest that the bone region of these scaffolds may have acceptable mechanical properties for

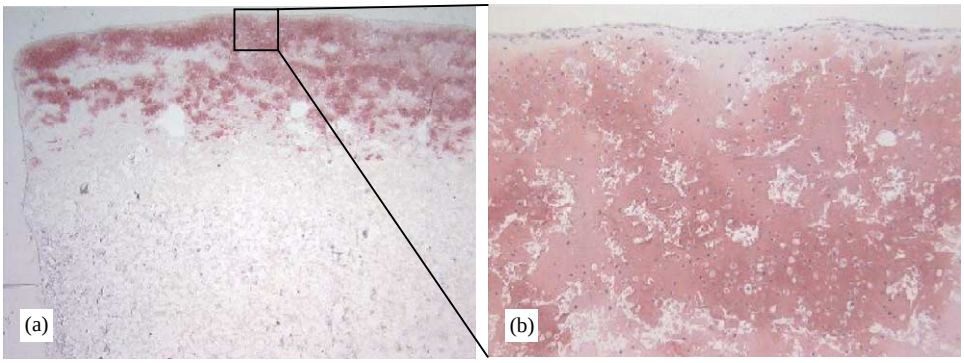

Fig. 8. Safranin-O-stained histological section of top seeded osteochondral scaffolds after 4 weeks in static culture at (a) 1.25× and (b) 10× magnification.

in vivo applications as a bone void filler. We acknowledge that the compressive properties of the chosen bone region of the scaffold are slightly lower than that of cancellous bone. However, it is not known what minimum strength is required for in vivo success of the scaffold, as the surrounding bone may provide protective support, and the scaffold will be invaded by new bone and remodeled while the scaffold continually degrades. It is likely that the mechanical strength of the scaffold will significantly increase with bone ingrowth [60]. If future in vivo studies demonstrate that the bone region is too weak, then the scaffold can be redesigned to have greater compressive properties by lowering the porosity and/or increasing the molecular weight (i.e., I.V.) of the polymers in the scaffold.

It is important to note that the properties shown here are for dry samples that had been exposed to aqueous solution only long enough to leach the salt. The mechanical properties at the time of implantation will be somewhat altered due to the aqueous environment, and potentially other factors such as swelling and loss of adhesion between the TCP and polymer particles. In addition, variables such as storage time and ambient conditions were not investigated, and these variables may influence the results.

The cloverleaf shape of the bone region was designed to allow adequate contact between the scaffold and surrounding bone in vivo for bone ingrowth but also leaves channels for bone marrow derivatives to contact a large surface area. This design was also created to be able to withstand torsional stress. It is important for the bone portion to be mechanically strong in order to withstand surgical implantation. Furthermore, the bone portion will ideally start to degrade during the bone ingrowth process. In addition to the incorporation of calcium phosphate, other osteoconductive and osteoinductive agents (e.g., BMPs) could be included.

The initial delamination seen between the cartilage and bone regions likely resulted from differential shrinkage of the two regions. It is has been reported that L-PLA has a glass transition temperature (T_g) of 57–65°C, and D,L-PLGA (50:50) undergoes a glass transition near 45–55°C. Scaffolds made with a 1:1 ratio of D,L-PLGA(50:50) and L-PLA have a T_g of approximately 53°C (unpublished data). Thus, it is unlikely that the shrinkage occurred due to plastic flow of the amorphous polymer while leaching at 37°C. These results suggest two possibilities: (1) the polymer in the device contains residual elastic strain around the NaCl particles which could be caused partially by collapse of the polymer (e.g., shrinkage of the overall dimensions of the device) when the supporting NaCl is leached out, or (2) the shrinkage was due to hydrostatic pressure.

In this device, a gradient of materials and porosity was used to overcome delamination. Delamination often occurs between regions where the material changes drastically, owing to the different physical properties of the materials (e.g., thermal expansion coefficient, elasticity, etc.) and structure of the regions (i.e., porosity). Using a gradient of materials and architectures, these physical properties were changed gradually, thereby preventing large discontinuities that could result in delamination. Using a gradient of materials was not enough to prevent delamination; it was also necessary to use a porosity gradient. Such gradients were easy to incorporate into the TheriForm process, which builds devices one layer at a time.

The high porosity of the cartilage region (90%) and low porosity of the bone region (55%) allowed the scaffolds to be fully submerged and exposed to chondrocytes during seeding, yet the chondrocytes preferentially attached to the cartilage region as desired. The unique macroscopic staggered channels in the cartilage portion of the device allowed chondrocytes to be seeded in vitro throughout the thickness of the device, not just on the top surface. This uniform seeding is important for rapid, homogeneous cartilage formation since chondrocytes cannot migrate easily over a large (2 mm) distance [33]. Thus, these staggered channels facilitated the direct seeding of chondrocytes into the center of the cartilage portion of the device. In addition, these channels allowed the transport of nutrients to the cells and removal of cellular by-products and polymer degradation by-products away from the cells during culture.

In summary, the TheriForm process has permitted the formation of a complex composite suitable as a cartilage-bone tissue engineered scaffold for implantation into articular defects. The versatility of the technology has allowed for a gradient of polymers, and various shapes and internal architectures to be incorporated. The mechanical testing and in vitro production of a cartilaginous matrix in the cartilage region of the scaffolds using chondrocytes suggest that these osteochondral devices have the potential to successfully repair articular defects in vivo. It is anticipated that this technology could be expanded to repair large regions of articular joints, and potentially whole joints for the treatment of osteoarthritis.

Acknowledgements

We would like to thank the following individuals for their involvement in this project: Brian Vacanti, Bugra Giritlioglu, Joe Berlingis, Hossam Hammad, Bill Rowe, Alice Yang, Joan Zeltinger, Ronda Schreiber, Kent Symons, and Leslie Rekettye.

References

[1] Park SH, Llinas A, Goel VK, Keller JC. Hard tissue replacements. In: Bronzino JD, editor. The biomedical engineering handbook, vol. 1, 2nd ed. Boca Raton, FL: CRC Press LLC, 2000. p. 44-1–35.

[2] American Academy of Orthopaedic Surgeons website: www.aaos.org.

[3] Buckwalter JA, Woo SL, Goldberg VM, Hadley EC, Booth F, Oegema TR, Eyre DR. Soft-tissue aging and musculoskeletal function. J Bone Joint Surg Am 1993;75(10):1533–48.

[4] Abdel-Rahman EM, Hefzy MS. Three-dimensional dynamic behaviour of the human knee joint under impact loading. Med Eng Phys 1988;20(4):276–90.

[5] Ahmed AM. The load-bearing role of the knee meniscus. In: Mow VC, Arnoczky SP, Jackson DW, editors. Knee meniscus: basic and clinical foundations. New York: Raven Press, 1992. p. 59.

[6] Atkinson PJ, Haut RC. Impact responses of the flexed human knee using a deformable impact interface. J Biomech Eng 2001;123(3):205–11.

[7] Engin AE, Tumer ST. Improved dynamic model of the human knee joint and its response to impact loading on the lower leg. J Biomech Eng 1993;115(2):137–43.

[8] Fukuda Y, Takai S, Yoshino N, Murase K, Tsutsumi S, Ikeuchi K, Hirasawa Y. Impact load transmission of the knee joint-influence of leg alignment and the role of the meniscus and articular cartilage. Clin Biomech 2000;15(7):516–21.

[9] Hoshino A, Wallace WA. Impact-absorbing properties of the human knee. J Bone Joint Surg Br 1987;69:807–11.

[10] Mow VC, Ratcliffe A, Poole AR. Review: cartilage and diarthrodial joints as paradigms for hierarchical materials and structures. Biomaterials 1992;13(2):67–97.

[11] Radin EL, de Lamotte F, Maquet P. Role of the menisci in the distribution of stress in the knee. Clin Orthop 1984;185:290–4.

[12] Schreppers GJ, Sauren AA, Huson A. A numerical model of the load transmission in the tibio-femoral contact area. Proc Inst Mech Eng [H] 1990;204:53–9.

[13] Walker PS, Erkman MJ. THe role of the menisci in force transmission across the knee. Clin Orthop 1975;109:184–92.

[14] Lapadula G, Iannone F, Zuccaro C, Grattagliano V, Covelli M, Patella V, Bianco G, Pipitone V. Chondrocyte phenotyping in human osteoarthritis. Clin Rheumatol 1998;17(2):99–104.

[15] Salter RB. The biological concept of continuous passive motion of synovial joints. The first 18 years of basic research and its clinical application. Clin Orthop 1989;242:12–25.

[16] Temenoff JS, Mikos AG. Review: tissue engineering for regeneration of articular cartilage. Biomaterials 2000;21:431–40.

[17] Buckwalter JA. Articular cartilage repair: injuries and potential for healing. J Orthop Sports Phys Ther 1998;28:192–202.

[18] Hangody L, Feczko P, Bartha L, Bodo G, Kish G. Mosaicplasty for the treatment of articular defects of the knee and ankle. Clin Orthop 2001;S391:S328–36.

[19] Attmanspacher W, Dittrich V, Stedtfeld HW. Experiences with arthroscopic therapy of chondral and osteochondral defects of the knee joint with OATS (Osteochondral Autograft Transfer System). Zentralbl Chir 2000;125:494–9.

[20] Jerosch J, Filler T, Peuker E. Is there an option for harvesting autologous osteochondral grafts without damaging weight-bearing areas in the knee joint? Knee Surg Sports Traumatol Arthrosc 2000;8:237–40.

[21] Cain EL, Clancy WG. Treatment algorithm for osteochondral injuries of the knee. Clin Sports Med 2001;20:321–42.

[22] Gao J, Dennis JE, Solchaga LA, Awadallah AS, Goldberg VM, Caplan AI. Tissue-engineered fabrication of an osteochondral composite graft using rate bone marrow-derived mesenchymal stem cells. Tissue Eng 2001;7(4):363–71.

[23] Mow VC, Ratcliffe A, Rosenwasser MP, Buckwalter JA. Experimental studies on repair of large osteochondral defects at the high weigh bearing area of the knee joint: a tissue engineering study. J Biomech Eng 1991;113:198–207.

[24] Paige KT, Vacanti CA. Engineering new tissue: formation of neocartilage. Tissue Eng 1995;1(2):97–106.

[25] Ahmad CS, Cohen ZA, Levine WN, Ateshian GA, Mow VC. Biomechanical and topographic considerations for autologous osteochondral grafting in the knee. Am J Sports Med 2001;29(2):201–6.

[26] Newman AP. Articular cartilage repair. Am J Sports Med 1998;26(2):309–24.

[27] Driesang IM, Hunziker EB. Delamination rates of tissue flaps used in articular cartilage repair. J Orthop Res 2000;18(6):909–11.

[28] O'Driscoll SW. Articular cartilage regeneration using periosteum. Clin Orthop 1999;S367:S186–203.

[29] Frenkel SR, Di Cesare PE. Degradation and repair of articular cartilage. Front Biosci 1999;4:D671–85.

[30] Schwartz RE, Grande DA. Cartilage repair unit. US Patent No. 5769899, 1998.

[31] Schaefer D, Martin I, Shastri P, Padera RF, Langer R, Freed LE, Vunjak-Novakovic G. In vitro generation of osteochondral composites. Biomaterials 2000;21(24):2599–606.

[32] Ameer GA, Mahmood TA, Langer R. A biodegradable composite scaffold for cell transplantation. J Orthop Res 2002;20(1):16–9.

[33] Freed LE, Marquis JC, Vunjak-Novakovis G, Emmanual J, Langer R. Composition of cell-polymer cartilage implants. Biotechnol Bioeng 1994;43:605–14.

[34] Freed LE, Martin I, Vunjak-Novakovic G. Frontiers in tissue engineering. In vitro modulation of chondrogenesis. Clin Orthop 1999;S367:S46–58.

[35] Martin I, Obradovic B, Treppo S, Grodzinsky AJ, Langer R, Freed LE, Vunjak-Novakovic G. Modulation of the mechanical properties of tissue engineered cartilage. Biorheology 2000;37(1–2):141–7.

[36] Athanasiou KA, Schitz JP, Agrawal CM. The effects of porosity on the in vitro degradation of polylactic acid-polyglycolic acid implants used in repair of articular cartilage. Tissue Eng 1998;4(1):53–63.

[37] Athanasiou KA, Korvick D, Schenck R. Biodegradable implants for the treatment of osteochondral defects in a goat model. Tissue Eng 1997;3(4):363–73.

[38] Freed LE, Marquis JC, Nohria A, Emmanual J, Mikos AG, Langer R. Neocartilage formation in vitro and in vivo using cells cultured on synthetic biodegradable polymers. J Biomed Mater Res 1993;23:11–23.

[39] Gugala Z, Gogolewski S. In vitro growth and activity of primary chondrocytes on a resorbable polylactide three-dimensional scaffold. J Biomed Mater Res 2000;49(2):183–91.

[40] Ishaug-Riley S, Okun LE, Prado G, Applegate MA, Ratcliffe A. Human articular chondrocyte adhesion and proliferation on synthetic biodegradable polymer films. Biomaterials 1999;20:2245–56.

[41] Obradovic B, Martin I, Padera RF, Treppo S, Freed LE, Vunjak-Novakovic G. Integration of enginered cartilage. J Orthop Res 2001;19(6):1089–97.

[42] Sachs E, Cima M, Williams P, Brancazio D, Cornie J. Three-dimensional printing: rapid tooling and prototypes directly from a CAD model. J Eng Ind 1992;114:481.

[43] Wu BM, Borland SW, Giordano RA, Cima LG, Sachs EM, Cima MJ. Solid free-form fabrication of drug delivery devices. J Controlled Rel 1996;40:77.

[44] Giordano RA, Wu BM, Borland SW, Cima LG, Sachs EM, Cima MJ. Mechanical properties of dense polylactic acid structures

fabricated by three-dimensional printing. J Biomater Sci Polym Ed 1996;8(1):63–75.
[45] Griffith L, Wu B, Cima ML, Powers MJ, Chaignaud B, Vacanti JP. In vitro organogenesis of liver tissue. Ann NY Acad Sci 1997;831:382.
[46] Kim YJ, Sah RL, Doong JY, Grodzinsky AJ. Fluorometric assay of DNA in cartilage explants using Hoechst 33258. Anal Biochem 1988;174:168–76.
[47] Schreiber RE, Dunkelman NS, Naughton G, Ratcliffe A. A method for tissue engineering of cartilage by cell seeding on bioresorbable scaffolds. Ann NY Acad Sci 1999;875:398–404.
[48] Schreiber RE, Ilten-Kirby BM, Dunkelman NS, Symons KT, Rekettye LM, Wiloughby J, Ratcliffe A. Repair of osteochondral defects with allogenic tissue engineered cartilage implants. Clin Orth Rel Res 1999;S367:S382–95.
[49] Farndale RW, Buttle DJ, Barrett AJ. Improved quantitation and discrimination of sulphated glycosaminoglycans by use of dimethylmethylene blue. Biochim Biophys Acta 1986;883:173–7.
[50] Dunkelman NS, Zimber MP, LeBaron RG, Pavelec R, Kwan M, Purchio AF. Cartilage production by rabbit articular chondrocytes on polyglycolic acid scaffolds in a closed bioreator system. Biotechnol Bioeng 1995;46:299–305.
[51] Woessner JF. The determination of hydroxyproline in tissue and protein samples containing small proportions of this amino acid. Arch Biochem Biophys 1961;93:440–7.
[52] Gibson LG, Ashby MF. Cellular solids: structure and properties, 2nd ed. Cambridge: Cambridge University Press, 1997.
[53] Saltzman WM. Transport in porous polymers. In: Brannon-Peppas L, Harland RS, editors. Absorbent polymer technology. Amsterdam: Elsevier, 1990. p. 171–99.
[54] White E, Shors EC. Biomaterial aspects of Interpore-200 porous hydroxyapatite. Dent Clin North Am 1986;30(1):49–67.
[55] Medpor product insert by Porex.
[56] Buckwalter JA, Glimcher MJ, Cooper RR, Recker R. Bone biology, I: structure, blood supply, cells, matrix, and mineralization. Instrum Course Lect 1996;45:371–86.
[57] Hulbert SF, Young FA, Mathews RS, Klawitter JJ, Talbert CD, Stelling FH. Potential ceramic materials as permanently implantable skeletal prostheses. J Biomed Mater Res 1970;4(3):433–56.
[58] Klawitter JJ, Bagwell JG, Weinstein AM, Sauer BW. An evaluation of bone ingrowth into porous high density polyethylene. J Biomed Mater Res 1976;10(2):311–23.
[59] Zeltinger J, Sherwood JK, Graham DA, Müeller R, Griffith LG. Effect of pore size and void fraction on cellular adhesion, proliferation, and matrix deposition. Tissue Eng 2001;7(5):557–72.
[60] Bieniek J, Swiecki Z. Porous and porous-compact ceramics in orthopedics. Clin Orthop 1991;272:88–94.